JOURNAL OF APPLIED PHYSICS **115**, 054501 (2014)

Influence of carbon content on the copper-telluride phase formation and on the resistive switching behavior of carbon alloyed Cu-Te conductive bridge random access memory cells

Wouter Devulder,[1,a)] Karl Opsomer,[2] Alexis Franquet,[2] Johan Meersschaut,[2] Attilio Belmonte,[2,3] Robert Muller,[2] Bob De Schutter,[1] Sven Van Elshocht,[2] Malgorzata Jurczak,[2] Ludovic Goux,[2] and Christophe Detavernier[1]
[1]*Department of Solid State Sciences, Universiteit Gent, Krijgslaan 281 (S1), 9000 Gent, Belgium*
[2]*IMEC, Kapeldreef 75, 3001 Leuven, Belgium*
[3]*KU Leuven, Department of Physics and Astronomy, Celestijnenlaan 200D, 3001 Leuven, Belgium*

(Received 16 October 2013; accepted 17 January 2014; published online 3 February 2014)

In this paper, we investigate the influence of the carbon content on the Cu-Te phase formation and on the resistive switching behavior in carbon alloyed $Cu_{0.6}Te_{0.4}$ based conductive bridge random access memory (CBRAM) cells. Carbon alloying of copper-tellurium inhibits the crystallization, while attractive switching behavior is preserved when using the material as Cu-supply layer in CBRAM cells. The phase formation is first investigated in a combinatorial way. With increasing carbon content, an enlargement of the temperature window in which the material stays amorphous was observed. Moreover, if crystalline phases are formed, subsequent phase transformations are inhibited. The electrical switching behavior of memory cells with different carbon contents is then investigated by implementing them in 580 μm diameter dot TiN/$Cu_{0.6}Te_{0.4}$-C/Al_2O_3/Si memory cells. Reliable switching behavior is observed for carbon contents up to 40 at. %, with a resistive window of more than 2 orders of magnitude, whereas for 50 at. % carbon, a higher current in the off state and only a small resistive window are present after repeated cycling. This degradation can be ascribed to the higher thermal and lower drift contribution to the reset operation due to a lower Cu affinity towards the supply layer, leading cycle-after-cycle to an increasing amount of Cu in the switching layer, which contributes to the current. The thermal diffusion of Cu into Al_2O_3 under annealing also gives an indication of the Cu affinity of the source layer. Time of flight secondary ion mass spectroscopy was used to investigate this migration depth in Al_2O_3 before and after annealing, showing a higher Cu, Te, and C migration for high carbon contents. © *2014 AIP Publishing LLC*.
[http://dx.doi.org/10.1063/1.4863722]

I. INTRODUCTION

Due to the continuous scaling down of memory devices, new memory concepts are investigated. Conductive bridge random access memory (CBRAM) seems a promising candidate, combining low power and fast operation with good scalability.[1] A typical CBRAM device consists of a Cu or Ag containing layer (cation supply layer), an insulating electrolyte layer, and an inert electrode. The cell can be switched to a low (LRS) or high resistive state (HRS) by, respectively, growing and dissolving a conductive filament in the electrolyte layer. Applying a positive potential on the cation supply layer induces filament growth through the insulating layer, switching the cell to a LRS when the filament bridges both electrodes, whereas a negative potential dissolves the filament again, switching the cell back to the HRS. For the insulating layer, chalcogenide materials[2–6] or binary metal oxides like HfO_2,[7] Ta_2O_5,[8] ZrO_2,[9] SiO_2,[10,11] and Al_2O_3[12] can be used. The latter being very promising due to high compatibility with the fabrication of complementary metal oxide semiconductor (CMOS) devices. Next to pure Cu or Ag as active electrode, alloys containing Cu have been reported.[13,14] Attractive memory properties have been demonstrated for the Cu-Te alloy,[14] and a strong influence of the Cu-Te composition on the switching properties of a Pt/Cu_xTe_{1-x}/Al_2O_3/Si memory cell was shown, with enhanced switching behavior in the range $0.5 < x < 0.7$[12] (henceforth referred to as $Cu_{0.6}Te_{0.4}$). However, the thermal stability of $Cu_{0.6}Te_{0.4}$ turns out to be limited, showing multiple phase transitions upon annealing.[15] For integration in a device, a material which is stable up to 400 °C is necessary.

In previous work,[16] we showed that addition of $\sim$40 at. % carbon to a Cu_xTe_{1-x} ($x \sim 0.6$) layer inhibited the crystallization of Cu-Te phases up to 360 °C. Carbon was chosen because it does not form a carbide phase with Cu or Te, and will not introduce new phases next to the copper telluride phases. Integrating this material in a 580 μm diameter, TiN/$Cu_{0.6}Te_{0.4}$-C/Al_2O_3/n+ Si memory cell showed attractive CBRAM functionality. This demonstrated the ability of carbon alloying to avoid the restructuring of the source layer. In this paper, we investigate the influence of the carbon content on the Cu-Te phase formation in the range of $\sim$0–45 at. % carbon. First, a combinatorial study is performed where the influence of the carbon content on the phase formation is investigated. Afterwards, the thermal stability and functionality as CBRAM source layer of a

a)Wouter.Devulder@UGent.be

 © 2014 AIP Publishing LLC

selection of carbon contents in the $Cu_{0.6}Te_{0.4}$ layer (hence referred to as $Cu_{0.6}Te_{0.4}$-C) are further studied.

II. EXPERIMENTAL

A combinatorial screening method was used to investigate the influence of the carbon content on the Cu-Te phase formation. A set of 150 mm Si wafers, covered by 100 nm thermal grown SiO_2 are mounted in a commercial physical vapor deposition tool with a base pressure of 5×10^{-7} mbar. The mixed Cu-Te-C layer is deposited by magnetron cosputtering of Cu, Te, and C from three different sputter targets. Shadow masks in front of the sputter targets allow for a spatial control of the material flux on the substrate, which gives the possibility to deposit a composition gradient along one direction on the wafer. This results in a deposited layer with a constant Cu/Te ratio and a gradient in the carbon content. There is an overall thickness gradient from ~66 (carbon poor) to ~36 nm (carbon rich), in agreement with the calculated thickness based on the deposition flux of each element through its shadow mask. The graded wafers are subjected to X-ray fluorescence spectroscopy (XRF) mapping, i.e., an XRF measurement is taken every 3 mm on the wafer in the composition gradient direction, to verify the Cu/Te ratio. This ratio was kept constant to 1.5, as this ratio showed enhanced switching behavior.[12] The gradient in carbon content on the other hand is calculated based on the deposited thickness of the Cu, Te, and C layers, using the elemental densities. The composition of the maximum carbon content was confirmed by Energy dispersive X-ray fluorescence spectroscopy (EDX).[16] This composition gradient was also confirmed by Rutherford backscattering spectroscopy (RBS) and Elastic recoil detection (ERD) to determine the Cu/Te and Cu/C ratio, respectively. Figure 1 shows the composition and the resistivity of the mixed Cu-Te-C layer: the Cu/Te ratio is constant and is equal to 1.5 and the carbon content increases from ~3 to ~45 at. %. The resistivity of the layer increases with increasing carbon content.

To investigate the influence of the carbon content on the Cu-Te phase formation, the graded wafers are annealed in a He atmosphere using a ramp anneal (5 °C/s) towards different temperatures and holding that temperature for 1 min. The crystallinity of the layer is investigated by X-ray diffraction (XRD). XRD-mapping (i.e., an XRD measurement is taken every 3 mm on the wafer, and hence at different carbon contents) of the wafers after annealing at different temperatures

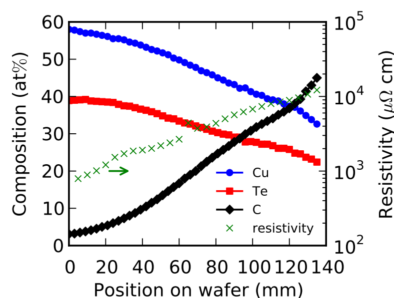

FIG. 1. Composition and resistivity of the mixed Cu-Te-C layer as a function of the position on the wafer. The Cu/Te ratio is fixed to 1.5 and the carbon content increases from ~3 to ~45 at. %.

gives an overview of the Cu-Te phases formed as a function of the carbon content and temperature.

A selection of compositions is investigated more in detail by means of *in situ* XRD. Here, the samples are heated in an inert He atmosphere at a constant heating rate of 0.5 °C/s and an XRD pattern in a fixed 2θ window is taken every 4 s. *In situ* XRD monitors the phase transformations that occur and hence gives information about the thermal stability.

The functionality of the $Cu_{0.6}Te_{0.4}$-C as CBRAM source layer for different carbon contents is investigated by integrating the material in 580 μm diameter TiN/$Cu_{0.6}Te_{0.4}$-C/Al_2O_3/n+ Si memory cells. These are created by subsequent magnetron sputtering of 50 nm $Cu_{0.6}Te_{0.4}$-C and 50 nm TiN through a dot shadow mask on a n+ Si substrate that is covered with a 3 nm Al_2O_3 layer. The Al_2O_3 is deposited by a H_2O based atomic layer deposition (ALD) process. The switching behavior is evaluated using a Keithley 2601A sourcemeter by applying a double linear voltage sweep from 0 to +3 V (and back) and from 0 to −3 V (and back), respectively, to set and reset the cell. The cycle speed was kept constant at 0.33 V/s and the current in the set operation was limited to 100 μA to protect the cell from breakdown.

The thermal diffusion and migration depth of Cu, Te, and C from the source layer into the Al_2O_3 under annealing conditions are also investigated and correlated with the electrical data. For this purpose, 10 nm $Cu_{0.6}Te_{0.4}(-C)$ was deposited on a 20 nm Al_2O_3/Si substrate and annealed for 30 min at 200 °C in He atmosphere. Depth profiles of Cu, Te, and C in the Al_2O_3 layer were measured with Time of Flight Secondary Ion Mass Spectrometry (ToF-SIMS) using a TOFSIMS IV instrument from ION-TOF GmbH. Both positive and negative ion profiles were measured in a dual beam configuration using a Bi_3^+ (25 keV) gun for analysis and a Xe^+ (500 eV) gun for sputtering.

III. RESULTS AND DISCUSSION

A. Combinatorial study

An XRD map is made for the as deposited wafer and after a 1 min anneal at 100, 200, 300, and 350 °C. An XRD θ-2θ measurement was taken every 3 mm along the gradient direction, and hence the XRD patterns could be correlated with the carbon content (see Figure 1). Figure 2 shows the XRD intensities plotted as a gray-scale color map as function of the carbon content for the as deposited wafer and after annealing at 200 and 350 °C. These maps are constructed for all annealing temperatures and allow us to identify most phases formed at discrete temperatures in the carbon range ~3 to ~45 at. %. A summary of the identified phases is depicted in Figure 3. Figure 2(a) shows for carbon contents lower than ~8 at. % the presence of the (003) and (006) peaks of hexagonal $Cu_{2-x}Te$[17] at, respectively, 12.3 and 24.7°. The absence of these peaks for higher C contents illustrates how addition of ~8 at. % carbon prevents the formation of polycrystalline Cu-Te phases already during deposition. The stoichiometry of the crystalline phase (2:1) is different from the 3:2 Cu:Te ratio, revealing also (non crystalline) Te rich regions in the as deposited layer. After

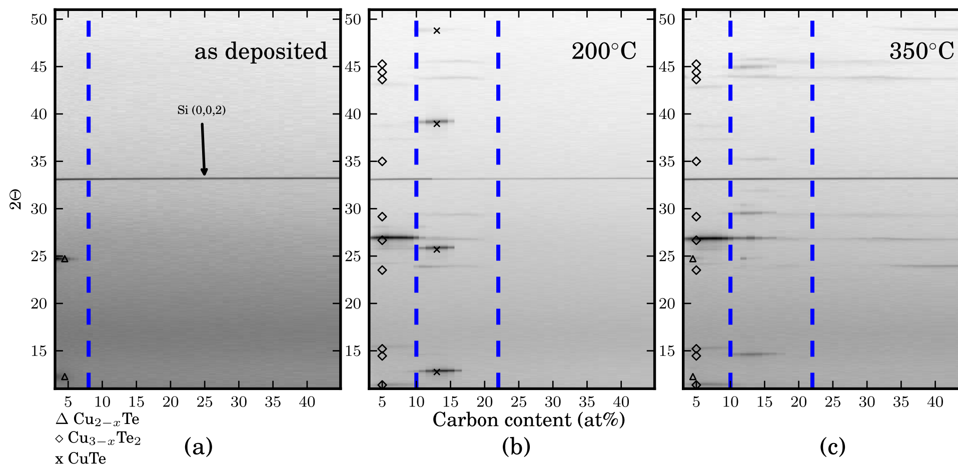

FIG. 2. XRD patterns of the graded $Cu_{0.6}Te_{0.4}$-C layer as a function of the carbon content for (a) the as deposited wafer and after 1 min anneal at (b) 200 and (c) 350 °C. The XRD intensities are plotted as a gray scale. The most prominent peaks of hexagonal $Cu_{2-x}Te$, orthorhombic $Cu_{3-x}Te_2$, and orthorhombic CuTe are indicated.

annealing at 100 °C, no significant difference with the as deposited sample is observed. At 200 °C, compositions with more than ~20 at. % C are still amorphous. In the 0–10 at. % C range, orthorhombic $Cu_{3-x}Te_2$[18] is observed: typical are the (021), (031), and (051) peaks at, respectively, 11.4, 15.2, and 23.5° (they do not exist for the higher temperature tetragonal $Cu_{3-x}Te_2$[19] phase which forms at ~172 °C[20]). In the 10–20 at. % C range, the (021) and (031) peaks are absent, but the (051) peak is detected, suggesting the orthorhombic phase. The (001), (002), (003), and (103) peaks of orthorhombic CuTe[21] are also clearly visible at, respectively, 12.8, 25.7, 38.9, and 48.8° for 10–17 at. % carbon. After annealing at 300 °C, no major differences are observed in the range 0–20 at. % C, only the (002), (004), and (006) peaks at, respectively, 14.5, 29.2, and 44.4° of orthorhombic $Cu_{3-x}Te_2$ are more apparent (and also at 350° in Figure 2(c)), whereas the (051) peak is fainter. The change in peak intensities suggests some preferred orientation, but can also be related to the tetragonal component of $Cu_{3-x}Te_2$, especially when the peaks that are typical for the orthorhombic phase can hardly be detected. For higher carbon contents, faint diffraction peaks of orthorhombic and/or tetragonal $Cu_{3-x}Te_2$ are now also observed. At 350 °C finally, $Cu_{2-x}Te$ is detected again in the range <8 at. %. In the 10–17 at. % C range, the CuTe signal is no more detectable, and only orthorhombic and/or tetragonal $Cu_{3-x}Te_2$ is observed.

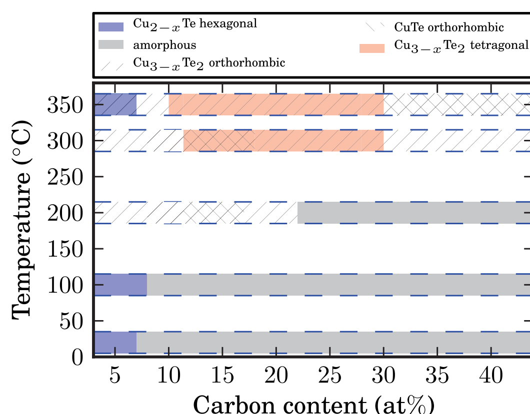

FIG. 3. The observed Cu-Te phases are shown for each annealing temperature as a function of the carbon content. These are determined from the observed XRD-peaks in the XRD-maps of the graded wafers.

To summarize this section, we obtained a crystalline as deposited $Cu_{0.6}Te_{0.4}$-C layer for carbon contents <8 at. %. In the range ~8–17 at. %, the layer is amorphous as deposited, but subsequent transformations occur under annealing. For higher C contents (>17 at. %), diffraction peaks of orthorhombic/tetragonal $Cu_{3-x}Te_2$ and orthorhombic CuTe (>30 at. %) are visible, and next to the amorphous-crystalline transition, no apparent transformations are observed. An increase in crystallization temperature is observed with increasing carbon content. In Sec. III B, the phase formation of $Cu_{0.6}Te_{0.4}$-C layers with a carbon content corresponding to each composition range is studied as a function of temperature using *in situ* XRD. This will give a clear view of the crystallization and subsequent phase transformation for each composition range.

B. Discrete compositions

Discrete samples with a constant layer thickness of 50 nm and with a Cu/Te ratio of 1.5 that contain ~10, ~20, and ~40 at. % carbon are deposited on 20 nm Al_2O_3. As a reference, a $Cu_{0.6}Te_{0.6}$ layer without carbon was also deposited. XRF measurements confirm for all samples a Cu/Te ratio close to 1.5. For the 20 and 40 at. % carbon samples, the carbon content was verified by EDX (respectively, 20.6 and 36.3 at. % C and a Cu/Te ratio of 1.52 and 1.6). In the case of 10 at. % carbon, the signal was too weak to determine the carbon content. The phase formation is investigated using *in situ* XRD. Figure 4 shows the result for the different compositions, confirming the general behavior that was observed in the combinatorial study.

In the case of pure $Cu_{0.6}Te_{0.4}$ (see Figure 4(a)), hexagonal $Cu_{2-x}Te$[17] is already formed during deposition. The 2:1 stoichiometry of the hexagonal phase is different from the 3:2 ratio that is expected from the composition, and hence more Te rich regions are also expected in the layer. These Te rich regions crystallize as orthorhombic CuTe[21] at 120 °C. Both phases react to tetragonal $Cu_{3-x}Te_2$[19] at 180 °C, but some CuTe is still present up to 350 °C. Finally, cubic $Cu_{2-x}Te$[22] is formed for $T > 400$ °C. For very low carbon contents in the combinatorial study, the (006) diffraction peak of $Cu_{2-x}Te$ at 24.7° was visible again after anneal at 350 °C, which is rather unexpected as for pure $Cu_{0.6}Te_{0.4}$,

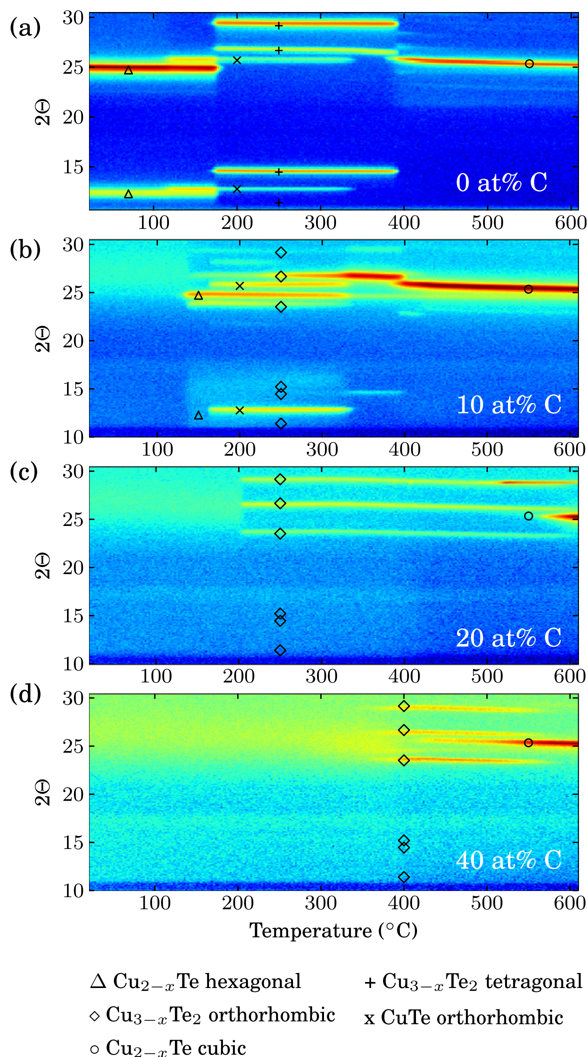

FIG. 4. *In situ* XRD pattern in the 10–30° window of a 50 nm $Cu_{0.6}Te_{0.4}$(-C) layer (a) without carbon, (b) with ∼10 at. % C, (c) with ∼20 at. % C, and (d) with ∼40 at. % C.

this phase does not appear in the *in situ* XRD pattern anymore after reaction with orthorhombic CuTe. The most plausible explanation is some left over that did not fully transform during the annealing of the combinatorial sample at 350 °C. Another observation was that cubic $Cu_{2-x}Te$ which is formed for $T > 400$ °C could not be quenched in and returns to the hexagonal form. This could also explain the occurrence of the hexagonal phase in the combinatorial study, although the cubic phase is not expected to be formed below 400 °C.

The combinatorial results demonstrated that a small amount of carbon could prevent the formation of any polycrystalline Cu-Te phase during deposition. Figure 4(b) illustrates this for a layer which contains ∼10 at. % carbon. Starting from an amorphous as deposited layer, hexagonal $Cu_{2-x}Te$ and orthorhombic $Cu_{3-x}Te_2$[18] are formed at 135 °C (in contrast to tetragonal $Cu_{3-x}Te_2$ as for pure $Cu_{0.6}Te_{0.4}$). Diffraction peaks of orthorhombic CuTe appear at 165 °C. These phases co-exist up to 330 °C, and then react to the high temperature tetragonal $Cu_{3-x}Te_2$[19] phase (i.e., the (051) peak of the orthorhombic lattice at 23.52° disappears whereas the (001) and (101) peaks of the tetragonal lattice at 14.5 and 26.7° become more apparent). As was already deduced from the combinatorial approach, still some transformations occur for this composition. However, it illustrates the role of the carbon: the crystallization and further transformations are inhibited.

Figure 4(c) shows the *in situ* measurement for a 20 at. % carbon alloyed $Cu_{0.6}Te_{0.4}$-C layer. The layer is amorphous up to 200 °C, and then orthorhombic $Cu_{3-x}Te_2$ and CuTe are formed (the (103) peak of CuTe at 48.8° is visible in the 30–50° 2θ window, but not shown here). Both phases co-exist and do not transform up to 560 °C. At higher temperatures, cubic $Cu_{2-x}Te$ is formed. In this way, a large temperature window where the material does not transform is created. This stabilizing effect can be explained by the fact that after crystallization of the Cu-Te phases, the carbon is most likely located at the grain boundaries of the Cu-Te crystals, making diffusion along the grain boundaries more difficult and hence impeding further transformations. This is further supported by the fact that no clear shift of the Cu-Te diffraction peaks is observed, indicating that the carbon atoms are not incorporated in the lattice, and hence are located outside the grains. This also strokes with the fact that no Cu and Te carbides are formed, as was verified by XPS.[16] In previous work,[16] we reported already that addition of ∼40 at. % carbon results in a material which is amorphous up to 360 °C. For completeness, this is also shown in Figure 4(d).

The results of the combinatorial study and the discrete samples invigorate our assumption that the inhibited crystallization is mainly related to kinetic aspects and the microstructure of the material. The combination of rather large elements like Cu and Te with a small element like C increases the packing density in the amorphous solid. This makes interdiffusion difficult, impeding the rearrangement in a crystalline structure and hence inhibiting the crystallization.[23] When more carbon is added, and hence with increased packing density, we observed an increase in the crystallization temperature. An increased thermal stability of amorphous alloys due to addition of small atoms like Be and C has been reported before.[24,25] The samples with ∼20 and ∼40 at. % carbon show attractive phase stability because of the large thermal window where no transformations occur.

C. Electrical characterization

The influence of the carbon content on the switching behavior of $TiN/Cu_{0.6}Te_{0.4}$-C/Al_2O_3/n+ Si CBRAM is investigated. Memory cells with 0, 20, 40, and 50 at. % carbon are prepared and the cells are cycled 20 times from which the set voltages are extracted. The resistance of the LRS and HRS state was measured by applying a read voltage of 20 mV after switching the cell on or off. Especially, the 20 and 40 at. % carbon samples are of interest, as these compositions have an improved thermal stability. Figure 5 shows the first and 20th cycle of a typical memory cell for every carbon content. The switching characteristics are very similar in the 0–40 at. % range (Figures 5(a)–5(c)). In the first

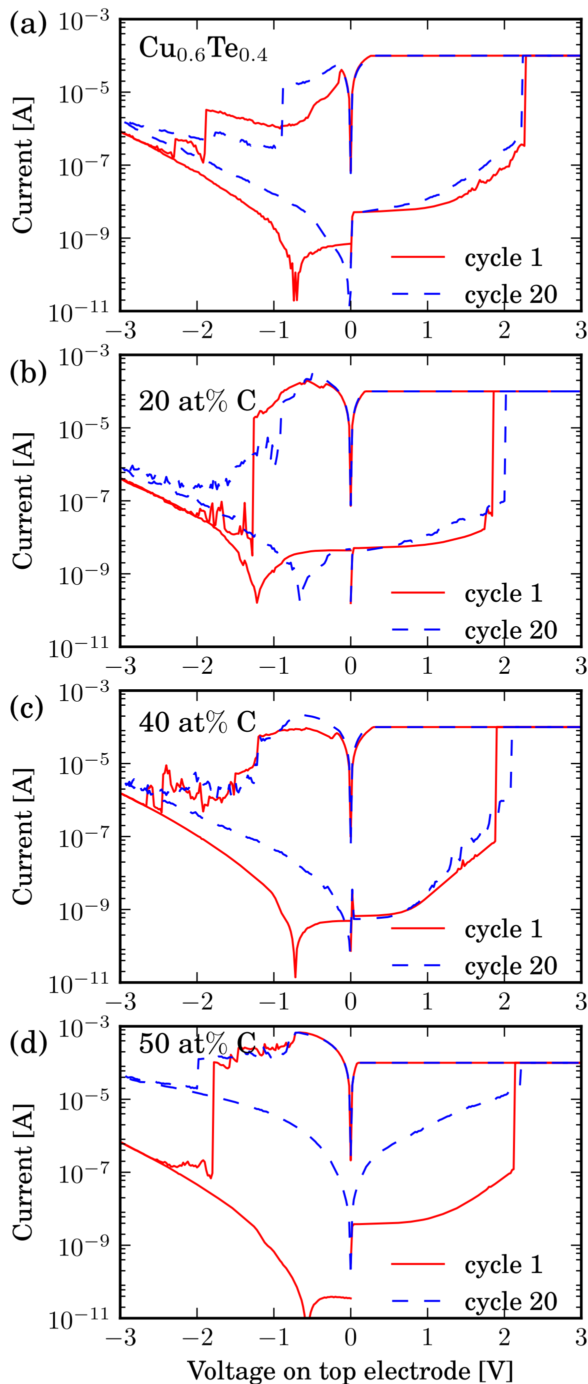

FIG. 5. Typical switching characteristics of a TiN/$Cu_{0.6}Te_{0.4}$(-C)/Al_2O_3/Si (50/50/3 nm) memory cell (a) without carbon, (b) with ∼20 at. % C, (c) with ∼40 at. % C, and (d) with ∼50 at. % C.

cycle, Cu is driven into the Al_2O_3 layer to form a conductive filament (e.g., the "forming" step). The subsequent IV traces and switching voltages are comparable with the first cycle, implying a complete filament erasure[26] and hence every cycle can be considered as a "forming" cycle. In the case of 50 at. % carbon (Figure 5(d)), a clear difference is observed between the first cycle and further switches. Whereas a deep reset could easily be achieved for lower carbon contents, for 50 at. % the cell does not return to the pristine HRS after a few cycles. This behavior could be described as switching where forming is observed (i.e., Cu is driven into the Al_2O_3 layer to form the filament and not all Cu is extracted again after reset).

A higher reset current is observed for the carbon alloyed memory cells, especially in the case of 50 at. % C. Both thermal effects and drift generally contribute to the reset operation.[26,27] The higher reset currents for the carbon alloyed cells suggest a more robust filament as higher currents are sustained. This will induce more Joule heating and hence the thermal component will have a larger contribution in the reset operation for carbon alloyed cells compared with pure $Cu_{0.6}Te_{0.4}$. The drift contribution on the other hand will be more important for the latter, evidenced by the low-current reset at already low voltages. This can be understood by a higher driving force for the Cu ions to go back to the supply layer due to the Cu-Te affinity, as pointed out before.[12] Consequently, the dominant thermal reset for the carbon alloyed cells might also suggest a lower Cu affinity towards the supply layer when more carbon is introduced, reducing the drift contribution. Furthermore, a different filament geometry (e.g., less conical for the carbon alloyed cells) can be present, inducing a more uniform field for the carbon alloyed cells during reset, which in turn leads to reduced drift and hence a thermal dominated reset.

Figure 6(a) compares the set voltage of the memory cells for different carbon contents, revealing a slightly lower set voltage for the carbon alloyed memory cells. This suggests an easier extraction of Cu from the carbon alloyed $Cu_{0.6}Te_{0.4}$ layers. We ascribe this to the amorphous nature of the Cu-supply layer, as the binding energy in a amorphous matrix is lower than in a lattice structure. Moreover, the dependence of switching parameters on binding energy of Cu in a fcc crystal and Cu-Te compounds has been pointed out before[12,28] and hence it is also reasonable to explain the observed difference between amorphous and crystalline source layers in this way. Remark that this easier extraction

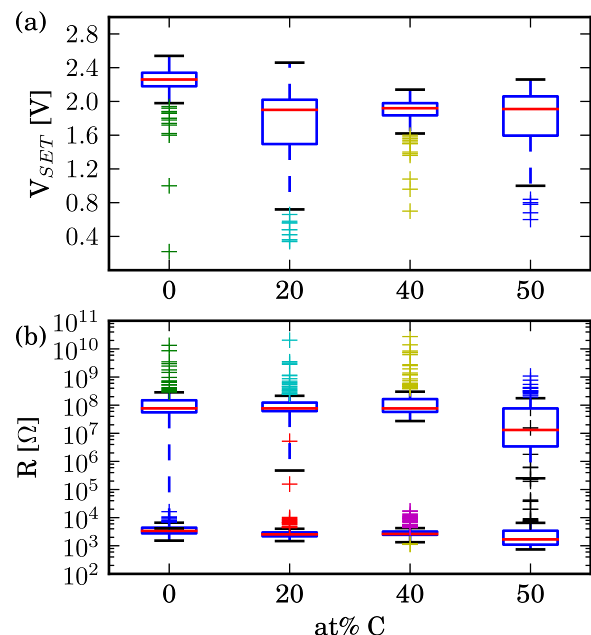

FIG. 6. (a) Set voltage and (b) resistance of the LRS and HRS of a TiN/$Cu_{0.6}Te_{0.4}$(-C)/Al_2O_3/Si (50/50/3 nm) memory cell for different carbon contents in the $Cu_{0.6}Te_{0.4}$(-C) layer. (Data from 10 devices × 20 cycles).

strokes with the proposed lower Cu affinity towards a carbon alloyed $Cu_{0.6}Te_{0.4}$ layer. Additionally, a more robust filament can be expected when the Cu ions are easier extracted from the supply layer, which is in agreement with the observed higher reset current. However, the lower set voltage may also be due to the presence of pure Cu. Small grains could be observed in HR TEM of a 40 at. % $Cu_{0.6}Te_{0.4}$-C layer,[16] and hence some pure fcc copper can be present here, without being detectable by XRD. The occurrence of pure Cu could also not be excluded from XPS measurements.[16] It is worth mentioning that with increasing carbon content, the resistivity of the $Cu_{0.6}Te_{0.4}$-C layer increases (see Figure 1), however no clear influence of the resistivity on the switching voltage is observed. This is to be expected as the resistivity of Al_2O_3 is orders of magnitude higher than $Cu_{0.6}Te_{0.4}$-C and hence the voltage will always drop over the Al_2O_3 layer.

The endurance was investigated by cycling the memory cells a 1000 times using the before mentioned programming sequence. Figure 7 shows the cumulative distribution of the LRS and HRS for memory cells with carbon contents from 0 to 50 at. %. It is clear that up to 40 at. % carbon, good endurance is observed with a resistive window of more than 2 orders of magnitude. For the cell with 50 at. % carbon, a similar resistive window is present in the first cycles, but after a few cycles, the HRS decreases and finally a small switch between LRS and HRS around a central value of $10^4\,\Omega$ is observed, resulting in a very small resistive window. Although, the presented switching curves for a memory cell with 50 at. % carbon (Figure 5(d)) remind of a forming behavior, the endurance tests reveal that the HRS further decreases and hence it should be considered as a degradation of the memory cell. The decrease in the resistance of the HRS is also already visible in Figure 6, showing the resistances of the HRS and LRS for all carbon contents. Whereas the LRS and HRS in the 0–40 at. % carbon range are very similar, for 50 at. %, a larger spread in the HRS is already observed. This behavior can be understood as a result of the lower Cu affinity towards the supply layer. The enhanced thermal and lower drift contribution might result in a significant lateral diffusion of Cu ions from the filament during reset (instead of going back to the source layer), which leads cycle-after-cycle to an increasing amount of Cu in the switching layer and contributes to the current in the HRS.

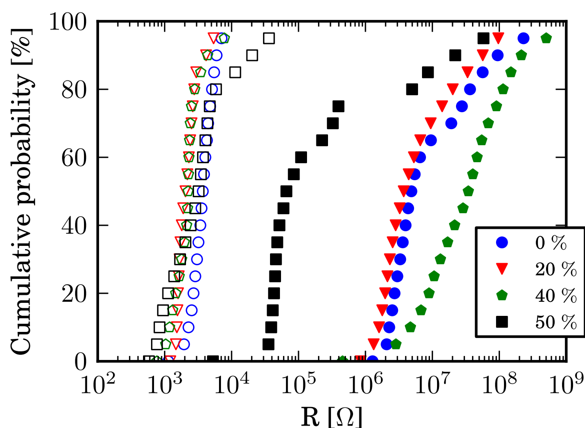

FIG. 7. Cumulative distribution of LRS (open markers) and HRS (filled markers) for 1000 cycles of a TiN/$Cu_{0.6}Te_{0.4}$-C/Al_2O_3/Si (50/50/3 nm) memory cell for different carbon contents.

D. ToF SIMS study

Next to a strong influence of carbon alloying on the Cu-Te phase formation, an influence on the switching behavior is observed. To investigate the extraction and diffusion of Cu more in detail, the diffusion of Cu into the aluminum oxide due to thermal activation is investigated. A 10 nm $Cu_{0.6}Te_{0.4}$(-C) layer with 0, 20, and 40 at. % carbon was deposited on a 20 nm Al_2O_3 layer and annealed for 30 min at 200 °C. A depth profile of the elements was performed with ToF SIMS for both the as deposited and annealed samples. Figure 8 shows the depth profile of the recorded Cu^+ and AlO^+ ions. The x-axis (sputter time) of each profile has been calibrated in depth (nm), setting the top of the Si signal at 30 nm. This assumes an identical sputter rate of both $Cu_{0.6}Te_{0.4}$(-C) and Al_2O_3 layers which is most likely not the case. With this calibration, the $Cu_{0.6}Te_{0.4}$(-C) layer is seen much thinner than expected. For pure $Cu_{0.6}Te_{0.4}$ (Figure 8(a)) and with 20 at. % (Figure 8(b)), a slight diffusion of Cu and Te (Te profile not shown) into the Al_2O_3 after annealing is observed, which is evidenced by the slope of the Cu^+ profile, and is in agreement with previous observations.[15] The profiles suggest a slightly larger diffusion depth in the case of pure $Cu_{0.6}Te_{0.4}$. Figure 8(c) depicts the profile for the sample with 40 at. % carbon and shows a much higher signal of Cu, Te, and C (Te and C not shown) in the Al_2O_3 layer after annealing compared with the sample without and with 20 at. % C. This illustrates, next to the electrical data, an easier extraction by thermal activation from the source layer and hence a lower Cu affinity for higher carbon

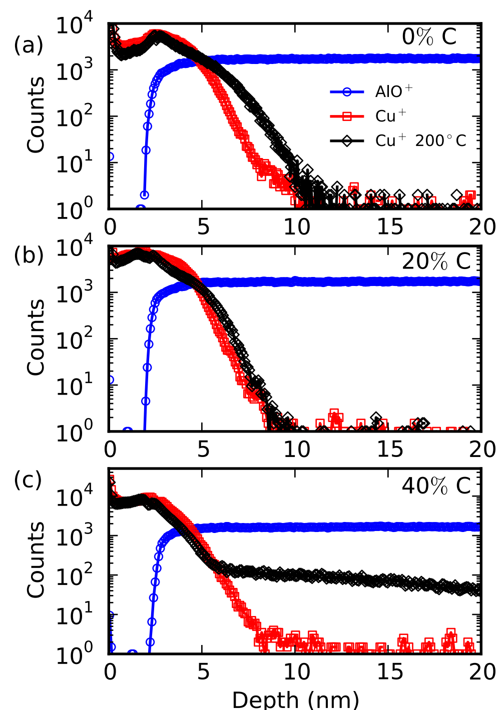

FIG. 8. Depth profile of Cu in the Al_2O_3 layer before and after anneal at 200 °C for (a) pure $Cu_{0.6}Te_{0.4}$ and with addition of (b) 20 at. % and (c) 40 at. % carbon.

contents. The ToF SIMS results suggest that with higher carbon contents, the elements are less tightly bound and—at least at the Al_2O_3 interface—can more easily be extracted from the supply layer. Although a clear signal is observed in the aluminum oxide, the actual amount of Cu is limited, as CBRAM functionality after this thermal treatment was still observed.

IV. CONCLUSIONS

In this paper, we investigated the influence of the carbon content in a Cu_xTe_{1-x} layer ($x \sim 0.6$) on the Cu-Te phase formation and on the switching behavior when integrating them as Cu-supply layer in 580 μm diameter dot CBRAM cells. Addition of ∼8 at. % carbon prevents already during deposition the formation of polycrystalline Cu-Te phases. Increasing the carbon content creates a larger temperature window where the material stays amorphous. Addition of 20 or 40 at. % carbon to the $Cu_{0.6}Te_{0.4}$ layer results in a material with a large temperature window where no phase transformations occur or with a large amorphous region, respectively. Both compositions show a good electrical switching behavior. A higher reset current is observed for the carbon alloyed memory cells compared with pure $Cu_{0.6}Te_{0.4}$. This suggests a larger contribution of thermal effects during reset operation, while a reduced drift contribution might point to a lower Cu affinity from the filament towards the supply layer. Addition of carbon also leads to a slightly lower set voltage, which we mainly attribute to the amorphous nature of the Cu-Te layer, where the Cu has a lower binding energy compared with a crystalline material. Increasing the carbon content to 50 at. % led to a degradation of the HRS after repeated cycling, i.e., a resistive window of only one order of magnitude is present. This degradation can be ascribed to the enhanced thermal and lower drift contribution to the reset operation, resulting in a significant lateral diffusion of Cu ions from the filament instead of going back to the source layer, which leads cycle-after-cycle to an increasing amount of Cu in the switching layer. The easier extraction and looser bounding structure of the elements with increasing carbon content were also confirmed by ToF SIMS depth profiling of Cu, Te, and C into Al_2O_3 after annealing a $Cu_{0.6}Te_{0.4}$-C/Al_2O_3/Si stack with different carbon contents. Higher diffusion of the elements into the oxide layer was observed when 40 at. % carbon was added compared with a 20 at. % carbon alloyed or a pure $Cu_{0.6}Te_{0.4}$ layer.

ACKNOWLEDGMENTS

This research was funded by a Ph.D. Grant of the Agency for Innovation by Science and Technology (IWT) and by the UGent-BOF GOA 01G01513.

[1]R. Waser, R. Dittmann, G. Staikov, and K. Szot, Adv. Mater. **21**, 2632 (2009).
[2]K. Terabe, T. Nakayama, T. Hasegawa, and M. Aono, Appl. Phys. Lett. **80**, 4009 (2002).
[3]T. Sakamoto, H. Sunamura, H. Kawaura, T. Hasegawa, T. Nakayama, and M. Aono, Appl. Phys. Lett. **82**, 3032 (2003).
[4]M. Kozicki, M. Park, and M. Mitkova, IEEE Trans. Nanotechnol. **4**, 331 (2005).
[5]M. Kund, G. Beitel, C.-U. Pinnow, T. Rohr, J. Schumann, R. Symanczyk, K.-D. Ufert, and G. Muller, *Tech. Dig. - Int. Electron Devices Meet., 5 December 2005*, (2005) p. 754.
[6]J. S. Kwak, E. J. Chi, J. D. Choi, S. W. Park, H. K. Baik, M. G. So, and S. M. Lee, J. Appl. Phys. **78**, 983 (1995).
[7]Y. Wang, H. Lv, W. Wang, Q. Liu, S. Long, Q. Wang, Z. Huo, S. Zhang, Y. Li, Q. Zuo, W. Lian, J. Yang, and M. Liu, IEEE Electron Device Lett. **31**, 1470 (2010).
[8]T. Tsuruoka, K. Terabe, T. Hasegawa, and M. Aono, Nanotechnology **21**, 425205 (2010).
[9]Q. Liu, S. Long, W. Wang, Q. Zuo, S. Zhang, J. Chen, and M. Liu, IEEE Electron Device Lett. **30**, 1335 (2009).
[10]C. Schindler, M. Weides, M. N. Kozicki, and R. Waser, Appl. Phys. Lett. **92**, 122910 (2008).
[11]Y. Bernard, V. T. Renard, P. Gonon, and V. Jousseaume, Microelectron. Eng. **88**, 814 (2011).
[12]L. Goux, K. Opsomer, R. Degraeve, R. Muller, C. Detavernier, D. J. Wouters, M. Jurczak, L. Altimime, and J. A. Kittl, Appl. Phys. Lett. **99**, 053502 (2011).
[13]S. Kim, M. Jo, J. Park, J. Lee, W. Lee, and H. Hwang, Electrochem. Solid-State Lett. **14**, H322 (2011).
[14]K. Aratani, K. Ohba, T. Mizuguchi, S. Yasuda, T. Shiimoto, T. Tsushima, T. Sone, K. Endo, A. Kouchiyama, S. Sasaki, A. Maesaka, N. Yamada, and H. Narisawa, *Int. Electron Devices Meet., 10–12 December 2007* (2007) p. 783.
[15]L. Goux, K. Opsomer, A. Franquet, G. Kar, N. Jossart, O. Richard, D. Wouters, R. Muller, C. Detavernier, M. Jurczak, and J. Kittl, Thin Solid Films **533**, 29 (2013).
[16]W. Devulder, K. Opsomer, F. Seidel, A. Belmonte, R. Muller, B. De Schutter, H. Bender, W. Vandervorst, S. Van Elshocht, M. Jurczak, L. Goux, and C. Detavernier, ACS Appl. Mater. Interfaces **5**, 6984 (2013).
[17]JCPDS Data Card No. 00-049-1411, International Centre for Diffraction Data, Newtown Square, PA (2004).
[18]JCPDS Data Card No. 00-026-1117, International Centre for Diffraction Data, Newtown Square, PA (2004).
[19]JCPDS Data Card No. 01-085-0606, International Centre for Diffraction Data, Newtown Square, PA (2004).
[20]A. Pashinkin and V. Fedorov, Inorg. Mater. **39**, 539 (2003).
[21]JCPDS Data Card No. 01-089-4311, International Centre for Diffraction Data, Newtown Square, PA (2004).
[22]JCPDS Data Card No. 00-045-1286, International Centre for Diffraction Data, Newtown Square, PA (2004).
[23]T. Zhang, A. Inoue, and T. Masumoto, Mater. Trans., JIM **32**, 1005 (1991).
[24]W. Wang, Q. Wei, and H. Bai, Appl. Phys. Lett. **71**, 58 (1997).
[25]W. Wang and H. Bai, J. Appl. Phys. **84**, 5961 (1998).
[26]L. Goux, K. Sankaran, G. Kar, N. Jossart, K. Opsomer, R. Degraeve, G. Pourtois, G. M. Rignanese, C. Detavernier, S. Clima, Y. Y. Chen, A. Fantini, B. Govoreanu, D. Wouters, M. Jurczak, L. Altimime, and J. A. Kittl, *IEEE Symp. VLSI Technol., 12–14 June 2012* (2012) p. 69.
[27]D. Ielmini, IEEE Trans. Electron Devices **58**, 4309 (2011).
[28]V. Afanas'ev, F. D. Stefano, M. Houssa, A. Stesmans, L. Goux, K. Opsomer, C. Detavernier, J. Kittl, and M. Jurczak, Thin Solid Films **533**, 34 (2013).

Journal of Applied Physics is copyrighted by the American Institute of Physics (AIP). Redistribution of journal material is subject to the AIP online journal license and/or AIP copyright. For more information, see http://ojps.aip.org/japo/japcr/jsp